Rayleigh-Taylor and Richtmyer-Meshkov instabilities in multilayer fluids with surface tension

Karnig O. Mikaelian
Lawrence Livermore National Laboratory, Livermore, California 94550
(Received 7 March 1990; revised manuscript received 27 July 1990)

Surface tension modifies the evolution of the Rayleigh-Taylor and the Richtmyer-Meshkov instabilities in fluids undergoing a constant acceleration or a shock, respectively. We analyze the general case of N fluids with arbitrary densities and surface tensions and derive the eigenvalue equation determining the growth rate of the perturbations. For $N=2$ we recover the classical case of two semi-infinite fluids and extend it to the case of two finite-thickness fluids between fixed boundaries. The $N=2$ case is studied in detail; we find universal modes that are independent of the thickness of the intermediate fluid, and we find how surface tension modifies Taylor's modes for a single fluid with free boundaries. We also analyze in detail recent and future two- or three-fluid experiments. Representing a shock as an impulsive acceleration we find that post-shock oscillations have frequencies and amplitudes that depend on the wave number k, leading to a nontrivial evolution for the spectrum of perturbations. Finally, we study turbulence at the interface between two fluids with surface tension and present specific predictions for the turbulent energy $E_{\text{turbulent}}$ as a function of the surface tension $T^{(s)}$. We propose new experiments, physical and/or numerical, to test our predictions.

I. INTRODUCTION

Interfaces between two fluids of different densities undergoing a constant acceleration or a shock are subject to Rayleigh-Taylor[1,2] (RT) or Richtmyer-Meshkov[3,4] (RM) instabilities. Perturbations of amplitude η grow exponentially or linearly in time: $\eta=\eta_0 e^{\gamma_{\text{RT}}\tau}$ or $\eta=\eta_0(1+\gamma_{\text{RM}}\tau)$ where $\gamma_{\text{RT}}=\sqrt{Akg}$, $\gamma_{\text{RM}}=\Delta v k A$, and $\tau=$time. These classical results apply to two semi-infinite fluids of densities ρ_1 and ρ_2 undergoing a constant acceleration g or an impulsive acceleration with an instantaneous jump in velocity given by Δv. The growth rates γ depend on the densities via $A=(\rho_2-\rho_1)/(\rho_2+\rho_1)$ and on the wavelength λ of the perturbations via $k=2\pi/\lambda$.

In this paper we study the effect of surface tension on RT and RM instabilities in fluids with arbitrary stratified density profiles (see Fig. 1). Bellman and Pennington[5] extended the two-fluid result to include surface tension $T^{(s)}$. We recover their results as a special case $N=2$ in our general treatment, which is a straightforward extension of our earlier N-layer matrix method.[6]

The primary effect of surface tension is to introduce a cutoff wave number k_c or, equivalently, a cutoff wavelength $\lambda_c=2\pi/k_c$, beyond which perturbations are stable:

$$k_c=[(\rho_2-\rho_1)g/T^{(s)}]^{1/2}=2\pi/\lambda_c \ .$$

The most dynamic variable in this expression is the acceleration g. For example, if we take $\rho_2-\rho_1\approx 1$ g/cm^3, $T^{(s)}\approx 10$ dyn/cm, and $g\approx g_0=980$ cm/s^2, then $\lambda_c\approx 0.6$ cm, which is relatively large. In practice the densities and surface tensions do not change by more than one or two orders of magnitude from the example quoted here, but the acceleration g can vary tremendously. In particular, the acceleration induced by a laser ablating material off a small target can reach 10^{16} cm/s^2 and therefore the cutoff wavelength λ_c is so small (~ 0.05 Å) as to be completely negligible.[7]

We have in mind applications other than inertial confinement fusion where such huge accelerations are found.[8] Examples where λ_c is not negligible include geophysical and laboratory applications. We are particularly interested in recent laboratory experiments[9,10] where the

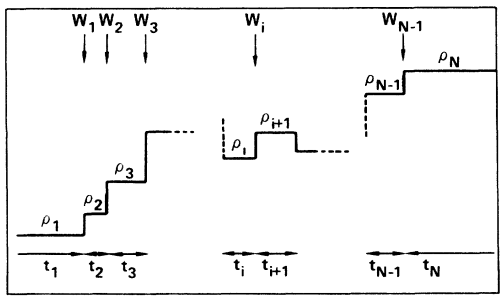

FIG. 1. Stratified density profile treated in this paper: N layers of fluids each with a constant density ρ_i and thickness t_i, $i=1,2,\ldots,N$. The first and last fluids are considered boundary fluids, i.e., $t_1=t_N=\infty$. W_i is the value of the perturbed velocity at interface i between fluids of density ρ_i and ρ_{i+1} and where the surface tension is $T_i^{(s)}$. The constant acceleration g is directed in the positive y direction, which is the direction of increasing i. The densities, thicknesses, and surface tensions are arbitrary; the W_i are eigenfunctions to be found by the eigenvalue equation, Eq. (4).

effect of surface tension is appreciable. A number of issues important to inertial confinement fusion, such as density-gradient stabilization, are studied in laboratory "water tank" experiments where the accelerations are necessarily small ($g \approx 5-50 g_0$) and therefore it is important to identify and account for the effect of surface tension in such experiments. In addition, a number of results found in this paper were unexpected, at least by us. We hope that new experiments will be carried out to verify them.

The plan of the paper is the following. In Sec. II we derive the general equations for arbitrary N. In Sec. III we consider the special case $N=2$, recovering the results of Bellman and Pennington and extending it to two fluids of finite thicknesses in a box. In Sec. IV we concentrate on the $N=3$ case and apply our analytic results to earlier or new experiments. In Sec. V we study the RM instability at an interface with surface tension, using methods pioneered by Richtmyer. In Sec. VI we investigate how surface tension affects the turbulent energy generated at the interface between two fluids. In the last section, Sec. VII, we review our results and present concluding remarks.

II. GENERAL RESULTS

We start with the second-order linear differential equation derived by Chandrasekhar:[11]

$$D(\rho DW) + \frac{gk^2}{\gamma^2} WD\rho - k^2 \rho W - \frac{k^4}{\gamma^2} \sum_i T_i^{(s)} \delta(y - y^i_+) W = 0 \ . \tag{1}$$

In this equation $W(y)$ is the perturbed velocity of the fluid having an arbitrary density profile $\rho(y)$, $T_i^{(s)}$ is the surface tension at interface i located at y^i_+, and D stands for the operator d/dy.

From Eq. (1) one obtains the jump conditions at an infinitesimally thin interface. Integrating Eq. (1) we obtain (see Ref. 11)

$$\Delta \left[\rho \frac{dW}{dy} \right] + \frac{gk^2}{\gamma^2} W \Delta\rho - \frac{k^4}{\gamma^2} T_i^{(s)} W = 0 \ , \tag{2}$$

where $\Delta(f) = f_+ - f_-$, f_+ and f_- referring to the values of f just above and below the interface, respectively.

We now apply Eqs. (1) and (2) to the case of N stratified fluids of constant but otherwise arbitrary densities $\rho_1, \rho_2, \ldots, \rho_{N-1}, \rho_N$ (see Fig. 1). Using the notation of Ref. 6, we let a fluid of density ρ_i and thickness t_i extend over the region $y^i_- \le y \le y^i_+$, so that $t_i = y^i_+ - y^i_-$. We will assume, as indicated in Fig. 1, that the first and last fluids act as boundary fluids and are infinitely thick, i.e., $t_1 \gg t_2$ and $t_N \gg t_{N-1}$. The interface between ρ_i and ρ_{i+1} is labeled i, so that $i = 1, 2, \ldots, N-1$, i.e., there are $N-1$ interfaces. The value of W at interface i will be denoted by W_i, $W_i \equiv W(y^i_+)$. Since the density is constant within each fluid region Eq. (1) reduces to $(D^2 - k^2)W = 0$, whose general solution is[6]

$$W = \frac{1}{S_i} \{ \sinh[k(y - y^i_-)] W_i + \sinh[k(y^i_+ - y)] W_{i-1} \} \tag{3}$$

within the range $y^i_- \le y \le y^i_+$, and where $S_i = \sinh(kt_i)$.

The general eigenvalue equations are obtained by requiring that the solutions W given in Eq. (3) satisfy the jump conditions given in Eq. (2) at each interface i. The algebra is straightforward and follows very closely Ref. 6. We find

$$\frac{1}{\rho_{i+1} - \rho_i - k^2 T_i^{(s)}/g} \left\{ -\frac{\rho_i}{S_i} W_{i-1} + \left[\rho_{i+1} \left[T_{i+1} + \frac{1}{S_{i+1}} \right] + \rho_i \left[T_i + \frac{1}{S_i} \right] \right] W_i - \frac{\rho_{i+1}}{S_{i+1}} W_{i+1} \right\} = \frac{gk}{\gamma^2} W_i \ , \tag{4}$$

where we have defined $T_i = \tanh(kt_i/2)$. For completeness and also for later use we write down Eq. (4) for the first ($i=1$) and last ($i=N-1$) interfaces, remembering that $t_1 = t_N = \infty$:

$$\frac{1}{\rho_2 - \rho_1 - k^2 T_1^{(s)}/g} \left\{ \left[\rho_2 \left[T_2 + \frac{1}{S_2} \right] + \rho_1 \right] W_1 - \frac{\rho_2}{S_2} W_2 \right\} = \frac{gk}{\gamma^2} W_1 \ , \tag{5a}$$

$$\frac{1}{\rho_N - \rho_{N-1} - k^2 T_{N-1}^{(s)}/g} \left\{ -\frac{\rho_{N-1}}{S_{N-1}} W_{N-2} + \left[\rho_N + \rho_{N-1} \left[T_{N-1} + \frac{1}{S_{N-1}} \right] \right] W_{N-1} \right\} = \frac{gk}{\gamma^2} W_{N-1} \ . \tag{5b}$$

Let us point out an interesting symmetry of the general matrix equation, Eq. (4). Since $T_i(-k) = -T_i(k)$ and $S_i(-k) = -S_i(k)$, Eq. (4) is symmetric under $k \to -k$. However, this is not true in general because the first and last equations, given above in Eqs. (5a) and (5b), respectively, clearly violate that symmetry, except when $\rho_1 = \rho_N = 0$. For fixed boundaries, we neglect the first and last equations, Eqs. (5a) and (5b), and use Eq. (4) with $i = 2, 3, \ldots, N-2$, setting $W_1 = W_{N-1} = 0$, which again restores the symmetry. We will refer to the symmetry property under $k \to -k$ as "parity." From the above discussion we conclude that all eigenvalues and eigenfunctions are symmetric under $k \to -k$, i.e., have even parity for *any* density profile as long as one or both of the boundaries are fixed or free. For finite-density boundary fluids ($\rho_1, \rho_N \neq 0$ or ∞), the symmetry does not hold. The reason is that one must require W to decay as $e^{-|ky|}$ in boundary fluids of finite density. Indeed, the differential equation, Eq. (1), as well as the resulting jump conditions, Eq. (2), are symmetric under $k \to -k$, and it is only boundary conditions that can violate such symmetry. Of course the classical $N=2$ case consists of just these two

"boundaries" and therefore is *not* symmetric under $k \rightarrow -k$.

In Ref. 6 we found analytic solutions for a continuous density profile $\rho = \rho_0 e^{\beta y}$ with a variety of boundary conditions. The solutions presented there for the fixed-fixed, fixed-free, free-fixed, and free-free cases all have even parity, but the case with fluid boundaries has no definite symmetry under $k \rightarrow -k$. This symmetry, which we had not noticed in Ref. 6, serves as a convenient check of any analytic or numerical solution, as we are using it here *a posteriori*.[12]

III. THE CASE $N=2$

This is the classical case of two semi-infinite fluids of densities ρ_1 and ρ_2 having a surface tension $T_1^{(s)}$ ($\equiv T^{(s)}$) at their common interface, which has sinusoidal perturbations of wavelength λ. Setting $i=1$ in the general eigenvalue equation, Eq. (4), and $T_{1,2}=1$, $S_{1,2}=\infty$, we get

$$\frac{1}{\rho_2-\rho_1-k^2T^{(s)}/g}(\rho_2+\rho_1)W_1=\frac{gk}{\gamma^2}W_1 ,$$

from which we derive the classical result[1,5]

$$\frac{\gamma^2}{gk}=\frac{\rho_2-\rho_1-k^2T^{(s)}/g}{\rho_2+\rho_1} . \tag{6}$$

Defining

$$k_c^2=\frac{(\rho_2-\rho_1)g}{T^{(s)}}=\left[\frac{2\pi}{\lambda_c}\right]^2 \tag{7}$$

Eq. (6) can be written as

$$\frac{\gamma^2}{gk_c}=A\left[1-\left[\frac{k}{k_c}\right]^2\right]\frac{k}{k_c} , \tag{8}$$

where A is the Atwood number, $A=(\rho_2-\rho_1)/(\rho_2+\rho_1)$.

For $k>k_c$ γ^2 is negative and therefore perturbations of wavelengths shorter than the cutoff wavelength λ_c ($=2\pi/k_c$) are stable. γ^2 vanishes at $k=0$ and k_c. In between, it reaches a peak value of

$$\frac{\gamma^2_{\text{peak}}}{gk_c}=\frac{2A}{3\sqrt{3}}\approx 0.38A \tag{9}$$

at $k^2=\frac{1}{3}k_c^2$ (see also Ref. 11).

Note the scaling in acceleration g: the peak value of the growth rate scales as $\gamma_{\text{peak}}\sim g^{3/4}$. This peak value is a relatively weak function of the surface tension, $\gamma_{\text{peak}}\sim(T^{(s)})^{-1/4}$. Away from the peak the effect of surface tension is negligible, the growth rate has the more familiar form $\gamma=\sqrt{gkA}$, and scales as $\gamma\sim g^{1/2}$.

In accordance with our discussion in Sec. II, Eq. (6) shows that γ^2 is not symmetric under $k\rightarrow -k$; in fact, it is antisymmetric, i.e., has odd parity.

If the two fluids have finite thicknesses t_1 and t_2 and are enclosed in a box, i.e., have fixed boundaries at $y=-t_1$ and $+t_2$ in a frame where $y=0$ marks the interface, then Eq. (6) is replaced by

$$\frac{\gamma^2}{gk}=\frac{\rho_2-\rho_1-k^2T^{(s)}/g}{\rho_2\coth(kt_2)+\rho_1\coth(kt_1)} , \tag{10}$$

where coth stands for the hyperbolic cotangent. Note that γ^2 is now symmetric under $k\rightarrow -k$, as expected from the discussion in Sec. II. Note also the stabilizing effect of the fixed boundaries: since the hyperbolic cotangent is always greater than 1, γ^2 in Eq. (10) is less than the γ^2 in Eq. (6). This effect, however, is noticeable only for extremely long-wavelength perturbations. For example, in a 1-cm-high water rank half full of water, the growth rate would be reduced by a factor of 1.8 for perturbations of wavelength $\lambda=10$ cm [$kt=\pi/10$, $\coth(\pi/10)\approx 3.3$].

IV. THE CASE $N=3$

A. Analytic results

For $N=3$ there are two interfaces and therefore the two eigenvalue equations are the "first" and "last" interface equations written explicitly in Eqs. (5a) and (5b), respectively. Since there is only one fluid (the middle one) that has a finite thickness, we will drop the subscripts and denote its thickness t_2 simply by t and similarly $T=\tanh(kt/2)$ and $S=\sinh(kt)$. The surface tensions at the first and second interfaces may be different, therefore we will keep our usual notation $T_1^{(s)}$ and $T_2^{(s)}$ for them.

Equations (5a) and (5b), with $N=3$, give the following two equations:

$$\frac{1}{\rho_2-\rho_1-k^2T_1^{(s)}/g}\times\left\{\left[\rho_2\left[T+\frac{1}{S}\right]+\rho_1\right]W_1-\frac{\rho_2}{S}W_2\right\}=\frac{gk}{\gamma^2}W_1 , \tag{11a}$$

and

$$\frac{1}{\rho_3-\rho_2-k^2T_2^{(s)}/g}\times\left\{-\frac{\rho_2}{S}W_1+\left[\rho_3+\rho_2\left[T+\frac{1}{S}\right]\right]W_2\right\}=\frac{gk}{\gamma^2}W_2 . \tag{11b}$$

By eliminating the ratio W_2/W_1 from the above two equations and defining $\chi\equiv\gamma^2/gk$ we get a quadratic equation for χ:

$$a\chi^2+b\chi+c=0 , \tag{12}$$

and therefore the two eigenmodes are given by

$$\chi_\pm=\frac{-b\pm(b^2-4ac)^{1/2}}{2a} . \tag{13}$$

The associated eigenfunctions are found by substituting the above $\chi_\pm$ in Eq. (11a) or (11b). Since the theory is linear, only the ratios $(W_2/W_1)_\pm$ are relevant, and they completely define the full eigenfunctions given in Eq. (3)

except, of course, for an overall normalization factor.

The coefficients a, b, and c in Eq. (12) are given by

$$
\begin{aligned}
a &= (1+ST)(\rho_3+\rho_1)+S(\rho_2+\rho_1\rho_3/\rho_2) , \\
b &= -(1+S+ST)(\rho_3-\rho_1)+\frac{Sk^2}{g\rho_2}(\rho_3 T_1^{(s)}+\rho_1 T_2^{(s)}) \\
&\quad +\frac{k^2}{g}(1+ST)(T_1^{(s)}+T_2^{(s)}) , \\
c &= S(\rho_3+\rho_1)-S(\rho_2+\rho_1\rho_3/\rho_2)-\frac{Sk^2}{g\rho_2}(\rho_3 T_1^{(s)}-\rho_1 T_2^{(s)}) \\
&\quad +\frac{Sk^2}{g}(T_1^{(s)}-T_2^{(s)})+\frac{Sk^4}{g^2\rho_2}T_1^{(s)}T_2^{(s)} .
\end{aligned}
\tag{14}
$$

We have several remarks to make and cases to consider.

(i) In Ref. 6, where we gave the above results without the surface tension terms, we pointed out that the eigenvalues possess an "inversion symmetry": the coefficients a, b, and c (and therefore $\chi_\pm$) are invariant under $\rho_2 \rightarrow \rho_1\rho_3/\rho_2$. For example, the profile $(\rho_1,\rho_2,\rho_3)=(1,5,10)$ has the same growth rates as the profile (1,2,10), and this is true for *any* wave number k. The surface tension terms *spoil* this symmetry.

(ii) With or without surface tension terms, the coefficients a, b, and c (and therefore $\chi_\pm$) possess no definite parity: under $k \rightarrow -k$ some terms change sign while others do not. Only when one of the interfaces is fixed and the other is free, or when both interfaces are free (clearly *both* interfaces cannot be fixed) do we obtain symmetry under $k \rightarrow -k$. For the fixed-free case ($\rho_1=\infty$, $\rho_3=0$) we get

$$
\frac{\gamma^2}{gk} = -\left[1+\frac{k^2 T^{(s)}}{g\rho_2}\right]/\coth(kt) , \tag{15}
$$

and for the free-fixed case ($\rho_1=0$, $\rho_3=\infty$) we get

$$
\frac{\gamma^2}{gk} = \left[1-\frac{k^2 T^{(s)}}{g\rho_2}\right]/\coth(kt) . \tag{16}
$$

In the above equations $T^{(s)}$ refers to the surface tension between the middle fluid and "vacuum." Clearly, γ^2 in these equations is symmetric under $k \rightarrow -k$, i.e., has even parity [this is no surprise—we obtained them from Eq. (10)].

The free-free case ($\rho_1=\rho_3=0$) deserves special treatment. Taylor[2] considered this case of a single fluid in vacuum without surface tension and we will see below [remark (vi)] how surface tension modifies his results.

(iii) To describe the general behavior of $\gamma_\pm^2$ we need a different approach from the one given earlier without surface tension.[6] In Ref. 6 we described $\chi_\pm$ as functions of ρ_2, the density of the middle layer, and this was possible because, without surface tension, their k dependence was uniform and our results were valid for arbitrary k. For example, we showed that χ_+ (χ_-) was minimum (maximum) when $\rho_2=\sqrt{\rho_1\rho_3}$.

The different approach is based on two key ideas: describe the k *dependence* of $\gamma_\pm^2$, and look for *zeros* of $\gamma_\pm^2$. We were somewhat surprised that despite the presence of several variables $(\rho_1,\rho_2,\rho_3,t,k,T_1^{(s)},T_2^{(s)})$ a general description is possible in this approach.

We first note the trivial zeros: $\gamma_\pm^2=gk\chi_\pm=0$ at $k=0$, i.e., infinitely long wavelengths have zero growth rates, with or without surface tension. The nontrivial zeros are located when $\chi_\pm=0$ or, equivalently, when $c=0$. From Eq. (14) we found that we could write c as

$$
c = S(k^2-k_{c1}^2)(k^2-k_{c2}^2)T_1^{(s)}T_2^{(s)}/g^2\rho_2 , \tag{17}
$$

where

$$
k_{c1}^2 = g(\rho_2-\rho_1)/T_1^{(s)} \tag{18a}
$$

and

$$
k_{c2}^2 = g(\rho_3-\rho_2)/T_2^{(s)} . \tag{18b}
$$

We therefore have no, one, or two nontrivial zeros depending on ρ_1, ρ_2, and ρ_3: there are no zeros if $\rho_1>\rho_2>\rho_3$, which we refer to as the stable-stable case. There are two zeros if $\rho_1<\rho_2<\rho_3$, an unstable-unstable case, and there is only one zero in the stable-unstable case when $\rho_1>\rho_2$ and $\rho_2<\rho_3$ (or $\rho_1<\rho_2$ and $\rho_2>\rho_3$). In Fig. 2 we show $\gamma_\pm^2$ as functions of k for these three cases. The cutoff wave number k_c indicated in Fig. 2 refers to the larger of k_{c1} and k_{c2}, i.e.,

$$
k_c^2 = \max\{k_{c1}^2,k_{c2}^2\} . \tag{19}
$$

The general behavior shown in Fig. 2 agrees with our intuitive expectations. The surprising aspect is that the cutoff wave numbers are given as though the interfaces were decoupled [see Eqs. (17) and (18)]. Even though γ_+ and γ_- are *not* given by $\gamma_{\text{classical}}(\rho_1,\rho_2)$ and $\gamma_{\text{classical}}(\rho_2,\rho_3)$, they share the *same* range of stability in k space. To illustrate their difference let us point out that unlike $\gamma_{\text{classical}}$, $\gamma_\pm$ do *not* peak at $k^2=\frac{1}{3}k_c^2$. Yet another way of expressing our surprise at Eqs. (17) and (18) is to point out that they are valid for any thickness t and that the dimensionless variable kt does not appear in the cutoff wave numbers.

The above points are illustrated numerically in Fig. 3 for the case $(\rho_1,\rho_2,\rho_3)=(1,3,9)$, so that the two local Atwood numbers are the same. This is true whenever $\rho_2=\sqrt{\rho_1\rho_3}$. We plot γ_+^2/gk_c and γ_-^2/gk_c in Figs.

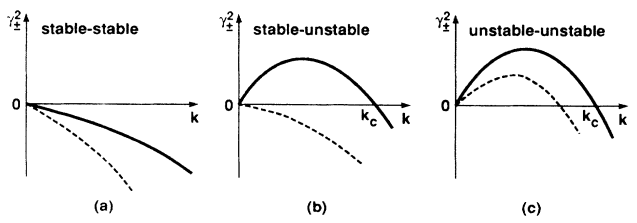

FIG. 2. General behavior of the two modes γ_+^2 (continuous curves) and γ_-^2 (dotted curves) for a 3-fluid system. There are three possible cases: (a) stable-stable, (b) stable-unstable, and (c) unstable-unstable.

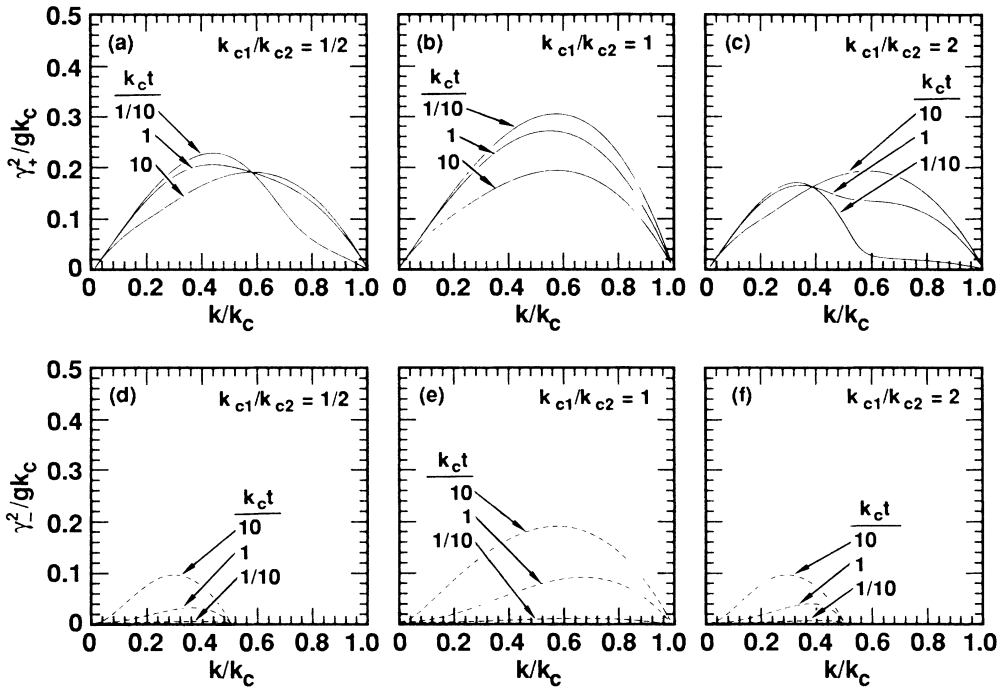

FIG. 3. For the case $(\rho_1,\rho_2,\rho_3)=(1,3,9)$ we plot $\gamma_\pm^2/gk_c$ vs k/k_c for $k_c t=0.1$, 1.0, and 10.0. k_c is the larger of the two cutoff wave numbers k_{c1} and k_{c2}, where $k_{ci}=[(\rho_{i+1}-\rho_i)g/T_i^{(s)}]^{1/2}$, and t is the thickness of the intermediate fluid of density ρ_2. The ratio k_{c1}/k_{c2} is indicated on each frame. The larger mode γ_+^2 is positive in the larger range $0<k<k_c$, while the smaller mode γ_-^2 is positive only in the smaller range $0<k<\min(k_{c1},k_{c2})$. "Universal points" appear when the curves intersect at one point and they correspond to wave numbers where γ_+ is independent of the thicknesses t, which happens in (a) and (c) at $k/k_c=1/\sqrt{3}$ and $1/\sqrt{7}$, respectively.

3(a)–3(c) and 3(d)–3(f) respectively. As defined in Eq. (19), k_c is the maximum of k_{c1} and k_{c2}, both of which are real for this unstable-unstable case. In each frame we give three curves showing the "thin" case ($k_c t=0.1$), the "intermediate" case ($k_c t=1$), and the "thick" case ($k_c t=10$). The ratio of the surface tensions is varied from frame to frame: as indicated on each frame, we have set $k_{c1}/k_{c2}=\frac{1}{2}$, 1, and 2 in Figs. 3(a), 3(b), and 3(c) respectively, and similarly for Figs. 3(d), 3(e), and 3(f). In the middle frames, Figs. 3(b) and 3(e), γ_+ and γ_- both vanish at $k=k_c=k_{c1}=k_{c2}$. In the side frames the larger modes vanish at $k=k_c$ while the smaller modes vanish at $k=k_c/2$.

As Fig. 3 shows, γ_+^2 and γ_-^2 are nontrivial functions of the wave number k and the thickness t: as the thickness is varied from thin ($k_c t=0.1$) to thick ($k_c t=10$), $\gamma_\pm^2$ vary substantially. However, they always vanish at the same point, independent of t. The thin case $k_c t=0.1$, shown in Fig. 3(c), is a particularly good example: the growth rate, after reaching its peak, is descending uniformly towards zero when it suddenly realizes that it cannot vanish until $k=k_c$, and therefore the curve is "stretched out" to make this destination. An explicit example of this behavior will be seen in our analysis of experiments.

(iv) As expected for short-wavelength perturbations $\lambda \ll t$, the interfaces decouple and the system behaves as two independent classical systems, i.e., $\gamma_\pm \to \gamma_{\text{classical}}$ with the appropriate local Atwood number and surface tension. This takes some nontrivial algebra if one tries to reduce Eqs. (13) and (14), but it is transparent from the original equations (11a) and (11b). The opposite limit of *long* wavelengths is more interesting. Clearly, as $kt \to 0$, $S \to 0$, $c \to 0$, and either γ_+ or γ_- (depending on the sign of b) vanishes. The nonvanishing mode is given by $\chi=-b/a$. From Eq. (14) $a \to \rho_3+\rho_1$, $b \to -\rho_3+\rho_1 +(k^2/g)(T_1^{(s)}+T_2^{(s)})$, and we get

$$\chi=\frac{\gamma^2}{gk}=\frac{\rho_3-\rho_1-(k^2/g)(T_1^{(s)}+T_2^{(s)})}{\rho_3+\rho_1} . \tag{20}$$

This expression agrees with the result $(\rho_3-\rho_1)/(\rho_3+\rho_1)$ given in Ref. 6 without surface tension. That result was quite uninteresting because it says that in this small kt limit, i.e., $\lambda \to \infty$ or $t \to 0$, the growth rate ignores the thin intermediate layer and behaves like the classical growth rate between two fluids of densities ρ_1 and ρ_3, which is not surprising. In the presence of surface tension, however, Eq. (20) shows that the growth rate "remembers" the middle layer through its surface tension even when $t \to 0$. An infinitesimally thin layer of intermediate fluid (surfactant) has no mechanical, i.e., density-related effect on the motion of the fluids, but it can substantially affect their stability through its surface tension. An explicit example will be given below when

we analyze water tank experiments.

Figures (3a) and (3c) exhibit another interesting aspect of this system which appears like a "triple point": at a specific value of k/k_c all three curves labeled $k_c t=0.1$, 1, and 10 go through the *same* point. This happens at $k/k_c=1/\sqrt{3}$ when $k_{c1}/k_{c2}=\frac{1}{2}$ [see Fig. 3(a)], and at $k/k_c=1/\sqrt{7}$ when $k_{c1}/k_{c2}=2$ [see Fig. 3(c)]. Actually, at these values of k/k_c the growth rates for *any thickness* t go through the same points, so that they are truly "universal points," i.e., the growth rates are independent of t. One may find universal points, if they exist, by setting $\partial\chi_{\pm}/\partial t=0$ (a complicated expression results) or, more simply, by equating the thin and thick limits of the growth rate. The points $k/k_c=1/\sqrt{3}$ and $1/\sqrt{7}$ quoted above were found in this way.

(v) The case $\rho_1=0$, $k_{c1}=k_{c2}=k_c$ is particularly interesting. Miraculous cancellations occur so that b^2-4ac becomes a perfect square, with the result

$$\frac{\gamma_+^2}{gk}=1-\frac{k^2}{k_c^2}\ , \tag{21a}$$

$$\frac{\gamma_-^2}{gk}=\left[1-\frac{k^2}{k_c^2}\right]\frac{(\rho_3-\rho_2)}{\rho_3\coth(kt)+\rho_2}\ . \tag{21b}$$

The surprising result is, or course, that the larger mode is *independent of t for all k*. As discussed in our previous remark, there can be universal points where γ_+ is independent of t. But those are at *specific* values of k: there is one such point in Fig. 3(a) and another one in Fig. 3(c). There is none in Fig. 3(b) where one perhaps would have expected it most. For the present case, however, independence from t extends over the *whole* range of k, i.e., we have complete universality.

To obtain $k_{c1}=k_{c2}$ the surface tensions must satisfy $T_2^{(s)}/T_1^{(s)}=(\rho_3-\rho_2)/(\rho_2-\rho_1)=\rho_3/\rho_2-1$, hence $\rho_3>\rho_2$. In the absence of surface tension ($k_c\to\infty$) Eqs. (21a) and (21b) reduce to our previous results.[6] Universality in that context becomes trivial because the mode in question, $\gamma^2=gk$, is present for all density profiles as long as one boundary is free and the other is not fixed ($\rho_1=0$, $\rho_N\neq\infty$). We can generalize our results to arbitrary N including surface tension as long as all the k_{ci} are equal and have the same common value k_c. In that case the eigenmode $\gamma^2=gk(1-k^2/k_c^2)$ associated with the pure eigenfunction $W=e^{-ky}$ is present, for (almost) any density stratification, if $\rho_1=0$ and $\rho_N\neq\infty$. In the opposite case, if $\rho_N=0$ and $\rho_1\neq\infty$, then the eigenmode that is always present is given by $\gamma^2=-gk(1+k^2/k_c^2)$ and is associated with the eigenfunction $W=e^{ky}$ (in both cases W decays exponentially away from the free surface). As in the tensionless case, these results follow from substituting the appropriate eigenfunctions $e^{\pm ky}$ in the general jump conditions, Eq. (2). The density profiles, however, are more restricted than the tensionless case because we must require positivity of $T_l^{(s)}$ which, as in the $N=3$ case discussed above, requires the densities to increase uniformly ($\rho_{i+1}>\rho_i$ if $\rho_1=0$ and $\rho_N\neq\infty$) or decrease uniformly ($\rho_{i+1}<\rho_i$ if $\rho_N=0$ and $\rho_1\neq\infty$). There is no such restriction for the tensionless case.

The above considerations will play an important role when we discuss Taylor's case, but the ramifications are quite general: as we showed in Ref. 6, without surface tension the two modes $\gamma^2=\pm gk$ are always present for any density profile between two free boundaries. With surface tension, quite the opposite happens: since such a density profile must necessarily increase at one boundary and decrease at the other, it cannot support universal modes.

(vi) Before studying Taylor's case in this last remark, let us quote our results for the slightly more general case of two identical boundary fluids, not necessarily vacuum. By setting $\rho_1=\rho_3$ and $T_1^{(s)}=T_2^{(s)}=T^{(s)}$ in Eqs. (13) and (14) we get

$$\frac{\gamma_{\pm}^2}{gk}=\frac{-[\rho_1+\rho_2\coth(kt)]\dfrac{k^2T^{(s)}}{g}\pm\left((\rho_1-\rho_2)^2\rho_{\text{eff}}^2+\dfrac{k^4\rho_2^2T^{(s)2}}{S^2g^2}\right)^{1/2}}{\rho_{\text{eff}}^2} \tag{22}$$

where $\rho_{\text{eff}}^2=\rho_1^2+\rho_2^2+2\rho_1\rho_2\coth(kt)$.

Dropping the surface tension terms we recover the result given in Ref. 6. A fair amount of algebra was needed to obtain the above equation, and the identity $ST^2+2T=S$ was used.

Finally, we set $\rho_1=\rho_3=0$ and obtain from Eq. (22) the extension of Taylor's case to include surface tension:

$$\frac{\gamma_{\pm}^2}{gk}=-\frac{k^2T^{(s)}}{g\rho_2}\coth(kt)\pm\left[1+\frac{k^4T^{(s)2}}{g^2S^2\rho_2^2}\right]^{1/2}\ . \tag{23}$$

Dropping the surface tension terms we recover Taylor's result[2] $\gamma_{\pm}^2/gk=\pm1$. Note that while Eq. (22) does not have a definite parity under $k\to-k$, this free-free case, Eq. (23), has even parity, as anticipated earlier in Sec. II.

We follow the general description given in our earlier remark (iii) to study the k dependence of $\gamma_{\pm}^2$. This is a stable-unstable case ($\rho_1<\rho_2$ and $\rho_2>\rho_3$), therefore the smaller eigenmode γ_-^2 is always negative—see Fig. 2(b). The larger mode γ_+^2 is positive in the range $0<k<k_c$ and it is negative beyond k_c where

$$k_c=(\rho_2 g/T^{(s)})^{1/2}\ . \tag{24}$$

In Fig. 4 we plot γ_+^2/gk_c as a function of k/k_c for a thin, intermediate, and thick layer, i.e., $k_c t=0.1$, 1, and 10, respectively.

This is perhaps the most striking difference between Eq. (23) and Taylor's result: with surface tension, the two eigenmodes depend on the thickness t; in contrast, when $T^{(s)}=0$, $\gamma_{\pm}^2=\pm gk$ for any t. In other words, there are no universal modes for the $\rho_1=\rho_3=0$ case with sur-

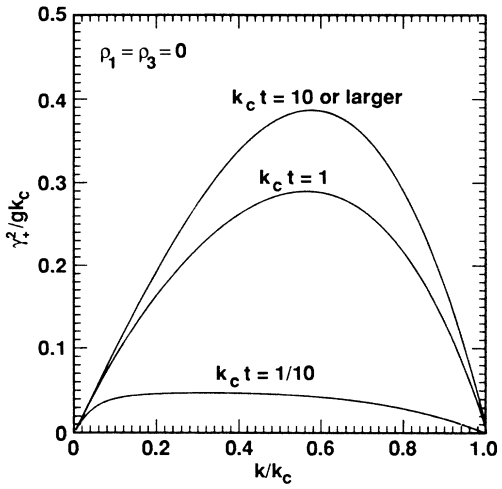

FIG. 4. For the case $\rho_1=\rho_3=0$ we plot γ_+^2/gk_c vs k/k_c for $k_c t=0.1$, 1.0, and 10.0. These curves are based on Eq. (23). γ_-^2 is negative for all k and is not shown. γ_+^2 becomes negative for $k>k_c$, where $k_c=[\rho_2 g/T^{(s)}]^{1/2}$. The curve labeled $k_c t=10$ or larger is given, to a very good approximation, by $\gamma_+^2/gk_c=[1-(k/k_c)^2]k/k_c$, which has a peak value of $2/3\sqrt{3}$ at $k/k_c=1/\sqrt{3}$.

face tension. Such behavior is expected from our previous discussion under remark (v): with surface tension, universal modes exist only if the density profile is uniformly increasing or decreasing, but this is not true when $(\rho_1,\rho_2,\rho_3)=(0,\rho_2,0)$. Without surface tension no such requirement is imposed on the density profile and, in fact, Taylor's modes $\pm gk$ are the two universal modes that are present for *any* density profile between two free surfaces with no surface tension. The requirement of a uniform density gradient is somewhat odd, but it is the reason why the eigenmodes with surface tension are given by Eq. (23) and *not* by $\pm gk-gk^3/k_c^2$ as one might have naively expected.

B. Experiments

We will analyze two recent experiments performed by Burrows, Smeeton, and Youngs[9] (BSY) and by Jacobs and Catton[10] (JC). Let us point out that neither experiment has so far measured the quantities we are interested in, viz., the growth rates of perturbations in their linear regime for three-fluid systems. The JC experiments have measured γ, but only for two fluids (we need three), while the BSY experiments have measured the turbulent mixing widths (we need γ's) for three fluids. Therefore most of the results given below are still predictions which, we believe, can be tested with only minor modifications to BSY or JC experiments. New water tank experiments have just gotten underway.[13]

We start with the BSY experiments[9] and in particular analyze experiment 73. The three fluids were (hexane, NaCl solution, carbon tetrachloride) with densities $(\rho_1,\rho_2,\rho_3)=(0.66,1.027,1.593)$ g/cm^3. These fluids were chosen because they satisfy $\rho_2\approx\sqrt{\rho_1\rho_3}$, and we had shown earlier that the larger growth rate is minimum when $\rho_2=\sqrt{\rho_1\rho_3}$ (in the absence of surface tension—see Ref. 6). The thickness of the intermediate layer, the NaCl solution, was $t=1$ cm. The surface tensions were $T_1^{(s)}=26$ dyn/cm and $T_2^{(s)}=22$ dyn/cm at the first and second interfaces, i.e., at the hexane-NaCl solution and at the NaCl-carbon tetrachloride interfaces, respectively. The effective acceleration was $g=46g_0$, where $g_0=980$ cm/s^2.

From the above data we find that $k_{c1}=25$/cm and $k_{c2}=34$/cm, hence the corresponding cutoff wavelengths are $\lambda_{c1}=0.25$ cm and $\lambda_{c2}=0.18$ cm. It is straightforward to show that the universal point is at $k/k_c\approx 0.77$, i.e., at $\lambda\approx 1.3\lambda_c\approx 0.23$ cm ($k_c=k_{c2}$). Since this lies between λ_{c1} and λ_{c2}, it follows that perturbations of wavelength 0.23 cm have only one unstable eigenmode γ_+ which, in addition, is independent of the thickness t. The result $k/k_c\approx 0.77$ was obtained by equating the thick result [i.e., $\gamma_{\text{classical}}$ as given in Eq. (8) with $A=0.22$) to the thin result given in Eq. (20). We also verified, numerically, that the growth curves for various thicknesses indeed pass through this point.

In Fig. 5 we plot γ_+ and γ_- as functions of the wavelength λ, using the experimental thickness $t=1$ cm. The purpose of that experiment was to assess the stabilizing effect of the intermediate layer (NaCl solution), hence we also show in Fig. 5 what the growth rate would have been without that intermediate layer, taking $T^{(s)}=50$ dyn/cm at the "ρ_1/ρ_3," i.e., hexane-carbon tetrachloride interface. Since $T_1^{(s)}+T_2^{(s)}=49$ dyn/cm, it is not surprising

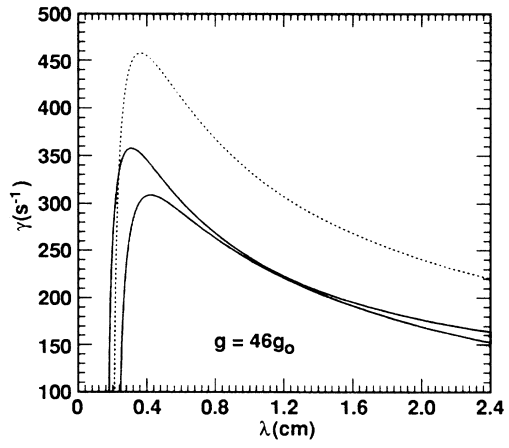

FIG. 5. For the 3-fluid experiment by BSY (Ref. 9) we plot the growth rates $\gamma_\pm$ per second as functions of perturbation wavelength in centimeters. These are shown by the two continuous curves. The experimental conditions are given by $(\rho_1,\rho_2,\rho_3)=(0.66,1.027,1.593)$ g/cm^3, $t=1$ cm, $T_1^{(s)}=26$ dyn/cm, $T_2^{(s)}=22$ dyn/cm, and $g=46g_0$ where $g_0=980$ cm/s^2. The dashed curve is a 2-fluid result where the middle layer of density ρ_2 has been removed.

that γ_+ (3-fluid) and γ(2-fluid) intersect close to the universal point $\lambda=0.23$ cm.

The stabilizing effect of the intermediate layer is clear from Fig. 5 where we see growth rates approximately 70% of classical, i.e., γ(3-fluid)$\approx$70%γ(2-fluid) for $\lambda \geq 0.3$ cm. This effect comes primarily from the reduced Atwood number: $A \approx 0.2$ in the 3-fluid case as compared with $A \approx 0.4$ for the 2-fluid case, that is

$$\frac{\gamma(\text{3-fluid})}{\gamma(\text{2-fluid})} \approx \left[\frac{A_{\text{3-fluid}}}{A_{\text{2-fluid}}} \right]^{1/2} \approx \frac{1}{\sqrt{2}} \approx 70\% \ .$$

As we mentioned earlier, the experimental observables were the turbulent mixing widths h_1 and h_2. The effect of the reduced Atwood number is in fact larger for h than for γ because $h \sim A$ while $\gamma \sim \sqrt{A}$. This stabilizing effect of the intermediate layer was seen in the experiments (see Ref. 9). The issue of turbulence will be taken up in Sec. VI.

We now turn to the JC experiments[10] where the growth rate was measured for a 2-fluid system, air-water. Since $\rho_{\text{air}} \approx 0$ and $\rho_{\text{water}} \approx 1$ g/cm^3, $A=1$ and the growth rate is given by $\gamma^2 = gk(1-k^2/k_c^2)$, where $k_c^2 = g\rho_{\text{water}}/T^{(s)}$. Experiments were carried out with $g=5g_0$ and $10g_0$. From Ref. 14, $T^{(s)}=72$ dyn/cm, and therefore the cutoff wavelengths are $\lambda_c=0.76$ and 0.54 cm for the $g=5g_0$ and $10g_0$ cases, which we show in Figs. 6(a) and 6(b), respectively. (As in Fig. 5 dashed lines are used for 2-fluid growth rates). Note that the peak values satisfy $\gamma_{\text{peak}}(10g_0)/\gamma_{\text{peak}}(5g_0) = 210/125 = 1.68 \approx 2^{3/4}$, in accordance with the $\gamma_{\text{peak}} \sim g^{3/4}$ scaling we discussed in Sec. III.

The experiments covered several wavelengths ranging from 0.8 to 5.1 cm and good agreement with theory was obtained for this classical $N=2$ system.[10] Strictly speaking, one must use the result for two finite-thickness fluids in a box, i.e., Eq. (10), for the air-water tank system, but since $\rho_{\text{air}} \approx 0$ and the water depth t_2 was 12.4 cm, the hyperbolic cotangent is very close to 1 even for the longest wavelength (5.1 cm).

We now discuss what happens if a thin layer of fluid is introduced at the original air-water interface, so that $N=3$ for the new system. For illustration we chose hexane, which satisfies the obvious experimental requirement that it be lighter than water (the static configuration must be stably stratified, i.e., $\rho_1 < \rho_2 < \rho_3$). Hence we have $(\rho_1,\rho_2,\rho_3) = (0.0, 0.66, 1.0)$ g/cm^3 and, from Ref. 14, $T_1^{(s)} = 18$ dyn/cm at the air-hexane interface and $T_2^{(s)} = 51$ dyn/cm at the hexane-water interface. Therefore $\lambda_{c1} = 0.47$ (0.33) cm and $\lambda_{c2} = 1.10$ (0.78) cm for $g=5g_0$ ($10g_0$). These cutoff wavelengths control the zeros of $\gamma_\pm$ for any thickness t of the intermediate layer (hexane in our example). For $t=0.01$, 0.05, and 0.10 cm we plot the corresponding γ_+ in Fig. 6(a) ($g=5g_0$) and Fig. 6(b) ($g=10g_0$). We do not show γ_-, the smaller growth rate, because it is much smaller than the larger growth rate.

The growth rates displayed in Figs. 6(a) and 6(b) have a nontrivial dependence on the thickness t and wavelength λ, particularly in the range $0.4 \leq \lambda \leq 0.8$ cm. At longer wavelengths all the growth rates approach the same value.

The "stretching" mentioned in our earlier remark (iii), necessary for γ_+ to vanish at $k=k_c$ and not before, is evident in these figures, particularly for the thin case ($t=0.01$ cm): in Figs. 6(a) and 6(b) we see that as γ_+ nosedives towards zero it is "pulled" sideways so as not to miss the mark $\lambda=\lambda_c$, beyond which it emerges as an imaginary number.

Unlike the BSY experiments (Fig. 5) where the intermediate layer reduces the growth rate γ, the intermediate layer here *increases* γ. The reason is the following: at short wavelengths the effects of surface tension are important and the smallness of $T_1^{(s)}$ at the air-hexane interface causes the instability. We know, from the general discussion given in remark (iii) earlier, that the larger mode cannot vanish before $k=k_c$ ($\lambda=\lambda_c$). From Fig.

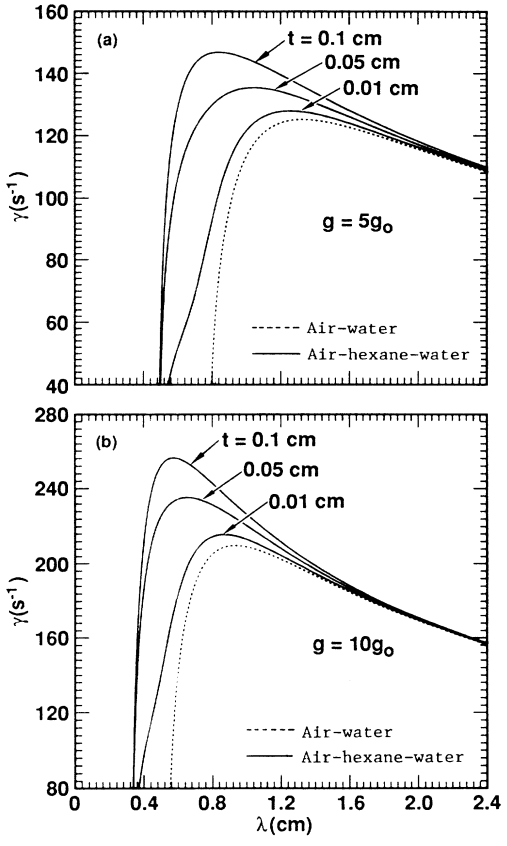

FIG. 6. Air-water experiments by JC (Ref. 10) with (a) $g=5g_0$ and (b) $g=10g_0$ where $g_0=980$ cm/s^2. The dashed curves give the growth rates per second as functions of perturbation wavelength λ in centimeters for the 2-fluid air-water case, $T^{(s)}=72$ dyn/cm. The continuous curves give the larger growth rate γ_+ (γ_- is negligible) for the case when an intermediate fluid, hexane, of thickness 0.1, 0.05, or 0.01 cm is introduced at the interface. This is a proposed 3-fluid air-hexane-water experiment in which the conditions will read $(\rho_1,\rho_2,\rho_3) = (0.0, 0.66, 1.0)$ g/cm^3, $T_1^{(s)}=18$ dyn/cm, $T_2^{(s)}=51$ dyn/cm, and thicknesses t and g as indicated on the figures.

6(a) [identical arguments apply, *mutatis mutandis,* to Fig. 6(b)] we expect γ_+ to still be finite in the vicinity of $\lambda=\lambda_c=0.47$ cm, while the $N=2$ air-water growth rate (dashed curve), having a large surface tension, vanishes at $\lambda=0.76$ cm and is imaginary (stable) at shorter wavelengths. This is best illustrated by the thinnest case $t=0.01$ cm. In short, the hexane layer acts as a surfactant reducing the air-water surface tension and, correspondingly, increasing the growth rate at short wavelengths.

At long wavelengths the effect of surface tension is negligible, but another principle prevents the hexane layer from stabilizing the system: as we showed in Ref. 6 and discussed in remark (v), when there is a free surface as in this case ($\rho_1=\rho_{\text{air}}\sim 0$), then the largest eigenmode $\gamma^2=gk$ is always present for *any* density profile as long as surface-tension effects are small, which they are at long wavelengths. In other words, in a regime where surface tension is negligible, one cannot use density gradient stabilization at a free surface. The stabilization achieved in the BSY experiments hinged critically on having a nonzero ρ_1 (one clearly cannot have the optimum density $\rho_2=\sqrt{\rho_1\rho_3}$ unless $\rho_1>0$). We should add, however, that as the wavelength of the perturbation gets longer and longer density gradient stabilization becomes less and less effective even with a nonzero ρ_1. For the BSY experiments this happens at wavelengths longer than the tank (15 cm). At such very long wavelengths the eigenmode reverts back to $\gamma^2=gk(\rho_3-\rho_1)/(\rho_3+\rho_1)$ as we discussed earlier [see the discussion following Eq. (20)].

The t dependence of γ_+ shown in Figs. 6(a) and 6(b) is nontrivial and perhaps worth measuring. With a slight modification it may be equally if not more interesting to verify the completely universal mode discussed in remark (v). Note that unlike the BSY experiments or the examples shown in Figs. 3(a) and 3(c) where universality occurred at a specific value of k, here we have either complete universality (independence form t for all k) or none at all.

To obtain complete universality we already satisfy the requirement of a uniformly increasing density profile: $\rho_1<\rho_2<\rho_3$. The remaining and crucial requirement is $k_{c1}=k_{c2}$. The natural surface tensions[14] do not accommodate this ($k_{c1}/k_{c2}=\lambda_{c2}/\lambda_{c1}\approx 2$), but one can easily change the situation by adding surfactants (this was done freely in BSY experiments and is a common practice). We make no specific suggestion here, except note that the resulting growth rate will be [Eq. (21a)]

$$\gamma_+^2=gk(1-k^2/k_c^2)$$

for any t and for whatever common value of k_c is achieved.

V. SHOCKS

Perturbations at the interface between two fluids can grow after the passage of a shock.[3,4] The growth is milder, being linear in time, as opposed to exponential growth when g is held constant. Shock-induced or Richtmyer-Meshkov instabilities have been studied[15] for fluids without surface tension (primarily gases). The extension from two fluids in N fluids, without surface tension, was done earlier.[16] In this section we incorporate the effects of surface tension, having primarily liquids in mind. We should point out, however, that in many shock tube experiments[4,15] a thin membrane is used to separate the two gases and this membrane acts like surface tension, hence our treatment may be relevant for this case also.

The description of the perturbations *after* the passage of the shock is fairly simple: from Eq. (6) it is clear that $\gamma^2<0$ if $g=0$, hence the perturbations will oscillate with time. Although this is the $N=2$ result, it is straightforward to show for any N that if $g=0$ then all the "growth rates" are imaginary and therefore the perturbations are all stable as long as $g=0$. Here we treat in detail the case $N=2$, i.e., the classical 2-fluid system with surface tension $T^{(s)}$. Since there are no thicknesses to be denoted by t, no confusion can arise if we change our convention in this section (and Sec. VI) by using the more common notation $t=$time.

The effect of the shock is to set up the "initial conditions" for the subsequent oscillatory behavior of the amplitude η:

$$\eta=\eta_0\cos(\omega t)+\frac{\dot{\eta}_0}{\omega}\sin(\omega t)\ , \tag{25}$$

where the frequency ω is given by Eq. (6) with $g=0$:

$$\omega=\left[\frac{k^3T^{(s)}}{\rho_2+\rho_1}\right]^{1/2}\ . \tag{26}$$

The values of η_0, $\dot{\eta}_0$, ρ_1, and ρ_2 are given by their postshock values. As Richtmyer showed, treating the shock as an instantaneous acceleration one obtains a simple result for $\dot{\eta}_0$ (which we will refer to as the "kick" imparted by the shock to the amplitude) and the results agreed well with his numerical calculations of fully compressible fluids.[3] We will continue to use this approach in the present case with surface tension.

The equation to be solved is

$$\frac{d^2\eta}{dt^2}=\gamma^2\eta=(gkA-\omega^2)\eta=[\Delta v\delta(t)kA-\omega^2]\eta\ , \tag{27}$$

where the impulsive acceleration is denoted by $g=\Delta v\delta(t)$, Δv being the jump in interface velocity imparted by the shock, and $\delta(t)$ is the Dirac delta function. In other words, an infinitely large acceleration acts for an infinitely short period of time resulting in a finite change in velocity.

The solution to Eq. (27) is given by Eq. (25) with

$$\dot{\eta}_0=\Delta vkA\eta_0\ , \tag{28}$$

which is obtained by integrating Eq. (27) over a very short period of time Δt bracketing the passage of the shock through the interface. Therefore

$$\eta=\eta_0\left[\cos(\omega t)+\frac{\Delta vkA}{\omega}\sin(\omega t)\right]\ . \tag{29}$$

Note that the effect of surface tension is to control the postshock oscillations only—it does not influence the

kick itself, which is given by Eq. (28). The reason is that during the shock the instantaneous acceleration is so large that any finite surface tension is ignored in generating the kick. If the surface tension, and hence ω, is very large, then Eq. (28) is replaced by the full result $\dot{\eta}_0=(\Delta v k A-\omega^2\Delta t)\eta_0$. Such an expression may be useful in modeling the effect of interfacial membranes in shock tube experiments, as we mentioned earlier.

Equation (28) represents the effect of the shock itself. In other words, the *change* in $\dot{\eta}$. If the derivative $\dot{\eta}(0_-)$ immediately before the shock is nonzero, then it must be added to it, i.e., we must let $\dot{\eta}(0)\rightarrow\dot{\eta}(0_+)=\dot{\eta}(0_-)+\Delta v k A\eta_0$ in Eq. (28).

If $T^{(s)}=0$, then $\omega=0$ and Eq. (29) gives Richtmyer's result $\eta=\eta_0(1+\Delta v k A t)$. Note that if $A<0$, the perturbation grows after changing phase, as was observed in Meshkov's experiments.[4]

The presence of surface tension leads to surprisingly interesting behavior. From Eq. (29) the amplitude oscillates in time with a maximum value given by

$$(\eta/\eta_0)_{\max}=\left[1+\left[\frac{\Delta v k A}{\omega}\right]^2\right]^{1/2} . \tag{30}$$

Note that $\Delta v k A/\omega$, the coefficient of the $\sin(\omega t)$ term in Eq. (29), is given by

$$\frac{\Delta v k A}{\omega}=\frac{\Delta v(\rho_2-\rho_1)}{[(\rho_2+\rho_1)kT^{(s)}]^{1/2}} . \tag{31}$$

In particular, this factor $\sim k^{-1/2}$, i.e., $\Delta v k A/\omega\sim\lambda^{1/2}$, and therefore long-wavelength perturbations have a large amplification factor η/η_0. However, $\omega\sim\lambda^{-3/2}$ [see Eq. (26)] and consequently such long-wavelength perturbations also take a very long time to reach their maximum. In the short run, shorter wavelengths may dominate. It is the λ dependence of $(\Delta v k A/\omega)\sin(\omega t)\sim\lambda^{1/2}\sin(\lambda^{-3/2})$ that leads to interesting evolution for $\eta(t)$.

From the above discussion it is clear that at any given time there is a wavelength of maximum or minimum amplification. We can find it by setting $\partial(\eta/\eta_0)/\partial k=0$, where the amplification factor η/η_0 is given in Eq. (29). It is convenient to define a "surface-tension speed" c_T by

$$c_T=\omega/k=\left[\frac{kT^{(s)}}{\rho_2+\rho_1}\right]^{1/2} , \tag{32}$$

in terms of which the amplification factor is

$$\eta/\eta_0=\cos(\omega t)+\frac{\Delta v A}{c_T}\sin(\omega t) . \tag{33}$$

Using the relations

$$\frac{\partial c_T}{\partial k}=c_T/2k, \quad \frac{\partial\omega}{\partial k}=3c_T/2 , \tag{34}$$

we can think of the perturbations as waves with a "phase speed" c_T and "group velocity" $\partial\omega/\partial k=3c_T/2$.

Using Eq. (29) or (33) we find that the requirement $\partial(\eta/\eta_0)/\partial k=0$ for an extremum leads to the following condition:

$$\tan(\omega t)=\frac{\omega t}{\frac{1}{3}+c_T\omega t/A\Delta v} . \tag{35}$$

This equation is a transcendental equation which, in general, must be solved numerically. There are infinitely many roots, and the maxima and minima alternate [this is seen by studying the second derivative $\partial^2(\eta/\eta_0)/\partial k^2$].

Note that the phase speed c_T is relatively small: for $\rho\sim1$ g/cm^3, $\lambda\sim1$ cm, $T^{(s)}\sim100$ dyn/cm, and $c_T\approx10$ cm/s. A shock can easily induce jump velocities Δv much larger than 10 cm/s. Equation (35) in this "strong shock" limit reduces to

$$\tan(\omega t)\sim3\omega t , \tag{36}$$

which can be solved approximately:

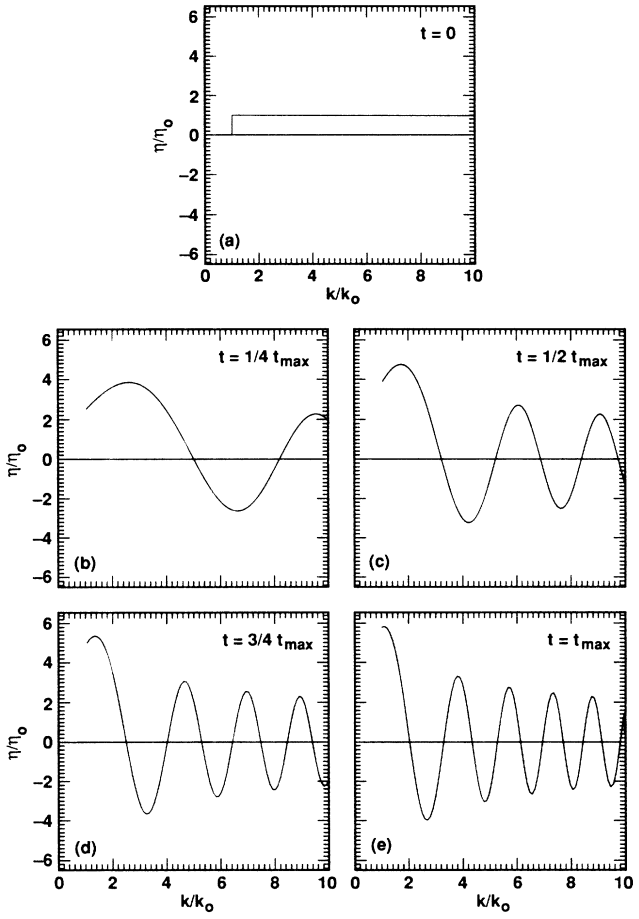

FIG. 7. Amplification factor η/η_0 for wave numbers in the range $1\le k/k_0\le10$ at five different times. An alternative interpretation is that η/η_0 represents the spectrum for a multiwavelength perturbation which is initially flat and evolves according to Eq. (29). The conditions read $A=1$, $\Delta v t_{\max}=\lambda_0=2\pi/k_0$, and $\omega_0 t_{\max}=1$, for which Eq. (29) reduces to

$$\eta/\eta_0=\cos[(k/k_0)^{3/2}t/t_{\max}]+2\pi(k_0/k)^{1/2}\sin[(k/k_0)^{3/2}t/t_{\max}].$$

The four "snapshots" are based on this equation. The time evolution of specific wavelength perturbations is shown in Fig. 8.

$$\omega t \approx 1.3 + n\pi \approx (\tfrac{5}{12} + n)\pi \ , \tag{37}$$

where $n = 0, 1, 2, \ldots$. As we mentioned above, the maxima and minima alternate. The first root, $\omega t \approx \frac{5}{12}\pi$, is a maximum.

We illustrate with an example, using Eq. (29) to plot the amplification factors for wave numbers over a range of one decade, i.e., $k_0 \le k \le 10k_0$. k_0 is a scale corresponding to the smallest wave number, i.e., the largest wavelength $\lambda_0 = 2\pi/k_0$ in the system. Next we define a time scale $t_{\max}$ by $\Delta v t_{\max} = \lambda_0$. It stands for the time needed to cover a distance λ_0 at the given jump velocity Δv. Finally, we set $A = 1$ and specify the surface tension via $\omega_0 t_{\max} = 1$, where ω_0 is given by Eq. (26) with $k = k_0$, i.e., $\omega_0^2 = k_0^3 T^{(s)}/(\rho_2 + \rho_1)$. Note that this is a relatively "weak shock" because $\Delta v / c_T = 2\pi\sqrt{k_0/k}$, which ranges between 2 and 6 for $1 \le k/k_0 \le 10$.

The amplification factors are shown in Fig. 7. The initial values are of course 1, i.e., at $t = 0$ $\eta/\eta_0 = 1$ for all k. Figures 7(b)–7(e) show η/η_0 at $t = \frac{1}{4}t_{\max}$, $\frac{1}{2}t_{\max}$, $\frac{3}{4}t_{\max}$, and $t_{\max}$ as functions of the wave number k in the range $k_0 \le k \le 10k_0$. The natural interpretation of Fig. 7 is clearly in terms of spectral evolution. At $t = 0$ we have a spectrum of perturbations that is flat, i.e., all perturbations have the same amplitude. The spectrum evolves as a function of time and Figs. 7(b)–7(e) represent snapshots of the spectrum as would be observed at $t = \frac{1}{4}t_{\max}$, etc. The evolution is fairly complex, though at any one time one can easily verify that the maxima and minima are given by Eq. (35). Note that by $t = t_{\max}$ most wavelengths have gone through several oscillations, but the longest wavelength has not quite reached its maximum.

Figure 7 also shows that the maxima of the longer wavelengths are larger than the maxima of the shorter wavelengths. In other words, an "envelope" joining the crests of the spectra in Fig. 7 would be a decreasing function of k/k_0. From Eqs. (30) and (32), the crests are given by

$$(\eta/\eta_0)_{\max} = \left[1 + \left[\frac{\Delta v A}{c_T}\right]^2\right]^{1/2}$$

and they asymptote to $1 + (\Delta v)^2 A^2 (\rho_2 + \rho_1)/2kT^{(s)} \to 1$ as $k \to \infty$, i.e., the very short-wavelength perturbations oscillate extremely fast but do not amplify.

In Fig. 8 we show the time evolution of three specific wavelength perturbations: $k = k_0$, $5k_0$, and $10k_0$. Note that the short-time behavior is indeed dominated by the short wavelengths, but the longest wavelength eventually wins over all others.

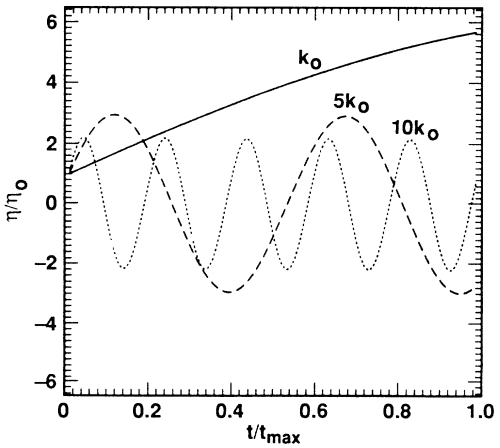

FIG. 8. Time evolution of η/η_0 for $k/k_0 = 1$, 5, and 10. The conditions are the same as in Fig. 7. Longer- (shorter-) wavelength perturbations oscillate slower (faster), but achieve larger (smaller) maxima.

VI. TURBULENCE

Unless special care is taken to set up a perturbation of a specific wavelength (this was done in the JC experiments[10] and in some of the BSY 2-fluid experiments[9,17]), natural surface finishes or thermal noise at fluid interfaces contain a continuous spectrum of perturbations. The nonlinear evolution of perturbations with such random initial conditions can best be described as the evolution of a mixing layer containing a mixture of the light ($\rho = \rho_1$) and heavy ($\rho = \rho_2$) fluids. So far quantitative results are available only from BSY experiments.[9,17] Denoting the mixing width into the heavier fluid by h, the experimental results can be summarized as

$$h = 0.07 A g t^2 \tag{38}$$

(t = time). Another experimental result, implicit in Eq. (38), is that h is independent of initial conditions. There is a relatively short time of transition from the initial linear regime (very small amplitudes) to the turbulent regime where Eq. (38) is applicable. Initial conditions appear to influence only this transition time and not the subsequent turbulent evolution. It is also observed that, as a function of time, longer and longer scales develop in the mixing layer.

These experiments used different fluids with different surface tensions, with or without surfactants added to change their surface tensions. The early weakly nonlinear behavior is consistent with the classical result [Eq. (8)] giving a most unstable wavelength at $\lambda = \sqrt{3}\lambda_c$, where λ_c is the cutoff wavelength defined in Eq. (7). The late-time turbulent behavior described by Eq. (38) is independent of surface tension, and this is consistent with the appearance of longer scales as the mixing evolves (the effect of surface tension is negligible at long wavelengths). The mixing width is controlled primarily by the appearance of these larger scales.

In addition to h the turbulent energy per unit mass $E_{\text{turbulent}}$ characterizes the mixing layer. There are, so far, no experimental measurements of turbulent energy, which is explained by the fact that $E_{\text{turbulent}}$ is more difficult (but not impossible) to measure than h. We have already presented our predictions for the tensionless case.[18] Here we take up the issue of how $E_{\text{turbulent}}$ depends on the surface tension $T^{(s)}$ or, equivalently, on λ_c.

Due to the nature of turbulence we doubt very much

that an answer can be found from first principles. We will therefore present only a model calculation, giving up the strict adherence to first principles used so far (Secs. I–V).

With this warning, we proceed to use the model of Canuto and Goldman[19] to calculate $E_{\text{turbulent}}$. There are several reasons for this recourse. First, the method of equating $E_{\text{turbulent}}$ to E_p, the potential energy lost in a gravitational field, which we proposed in Ref. 18 and applied to the tensionless case, is not useful here—with surface tension, some of the E_p goes into surface stretching and only the rest converts to turbulent energy. Unless we have an estimate for $E_{\text{surface tension}}$ in the mixed layer, we cannot use this (potentially more reliable) principle. Second, in Ref. 18 we also used the Canuto-Goldman model to calculate the tensionless $E_{\text{turbulent}}$, so that the calculation presented here can be compared directly with it. Of course, in the limit $T^{(s)}\rightarrow 0$ the two results have to match. Finally, the Canuto-Goldman model is well suited for our purpose, which is to describe how $E_{\text{turbulent}}$ is affected by $T^{(s)}$; the model involves the growth rate γ explicitly so that any modification to γ is directly incorporated in $E_{\text{turbulent}}$.

We have already used the Canuto-Goldman model for a similar purpose.[20] Ablation on a laser driven target reduces the growth rate γ and in Ref. 20 we used the same model to find out how $E_{\text{turbulent}}$ is reduced in response to ablative stabilization. We refer to this work not just to cite an example of how the model can be used, but also to reveal an additional reason for studying surface tension in general. The reduction in γ coming from ablative stabilization is mathematically similar to surface tension stabilization, with v_{ablation}^2/g playing the role of the cutoff wavelength λ_c. By studying how single wavelength perturbations and turbulent energy respond to surface-tension stabilization we hope to increase our understanding of ablative stabilization.

The model was derived assuming isentropic turbulence and therefore does not include explicitly the reverse mode cascading seen in the experiments: larger eddies evolving from the initial small eddies. Our approach to this problem has been to make λ_0 a function of time, where λ_0 is a parameter in the model (see below) representing the largest eddy in the system. The time evolution of λ_0 is not determined within the model. To find $\lambda_0(t)$ we have compared $E_{\text{turbulent}}$ in the Canuto-Goldman model with the E_p lost in a gravitational field,[18] valid strictly for $T^{(s)}=0$. From our analysis of this tensionless case, which we mention briefly at the end of this section, one can conclude that the model is consistent with (though by no means predicts) reverse cascading. Comparisons with other models will no doubt be highly interesting.

For completeness we repeat here the equations of the model:[19]

$$E_{\text{turbulent}}(k_0,k_c)=\int_{k_0}^{k_c} F\,dk \ , \tag{39}$$

where the spectrum $F(k)$ is found from the following equation:

$$-2\Gamma F=\frac{1}{k^2}\frac{d}{dk}\left[k\gamma^{1/2}\int_{k_0}^{k}k\gamma^{1/2}\frac{d}{dk}\left[\frac{\gamma}{k^2}\right]dk\right] , \tag{40}$$

in which the constant Γ is given by

$$\Gamma^{-1}=-\frac{k_0L_p^{-2}}{2\gamma(k_0)}\frac{d}{dk}\left[\frac{\gamma}{k^2}\right]_{k=k_0} , \tag{41}$$

with the longitudinal scale L_p defined by (see, e.g., Ref. 21)

$$L_p=\left[\frac{3\pi}{4}\right]\left[\int\frac{F}{k}dk\Big/\int F\,dk\right] . \tag{42}$$

The lower limit of integration k_0 corresponds to the minimum wave number (i.e., largest wavelength $\lambda_0=2\pi/k_0$) present in the system. The upper limit k_c is the cutoff wave number given in Eq. (7) for this particular case of the growth rate γ, which is given in Eq. (8). From the form of γ and a simple dimensional argument we immediately infer that $E_{\text{turbulent}}=Ag/k_0$ times a function of k_c/k_0. The tensionless case is given by $T^{(s)}\rightarrow 0$, i.e., $k_c/k_0\rightarrow\infty$.

Given A, g, k_0, and k_c, the model equations Eqs. (39)–(42) determine $E_{\text{turbulent}}$ completely without any additional parameters. We should add that this property of the model, viz., being free of arbitrary adjustable constants, is a fourth and important reason for using it, in addition to the three mentioned above.

Unlike the ablative case, we could not carry out the integrations analytically—the form of γ is different here. Therefore we will present our results numerically. This is not a severe handicap given the scaling discussed above: $E_{\text{turbulent}}=Ag/k_0f(k_c/k_0)$, and we need determine only one universal function f of (k_c/k_0).

Our result is shown in Fig. 9 as the curve labeled $\gamma^2/gkA=1-k^2/k_c^2$. Of course, $E_{\text{turbulent}}=0$ if $k_c=k_0$. In the opposite limit (tensionless) where $k_c/k_0\rightarrow\infty$ the result is

$$E_{\text{turbulent}}=\frac{2}{3}\left[\frac{56}{9\pi}\right]^2\frac{Ag}{k_0}\quad(T^{(s)}=0) . \tag{43}$$

Equation (43) represents an upper limit on $E_{\text{turbulent}}$. For example, if $A=1$, $g=980$ cm/s^2, and $k_0=1$ cm^{-1} ($\lambda_0=2\pi$ cm), then $E_{\text{turbulent}}\approx 2563$ ergs/g.

The effect of surface tension on $E_{\text{turbulent}}$ is twofold: (i) it reduces γ from $\gamma^2/gkA=1$ to $\gamma^2/gkA=1-k^2/k_c^2$, and (ii) it reduces the integration region from $k_0\le k\le\infty$ to $k_0\le k\le k_c$. To separate these two effects we show in Fig. 9 a second curve in which we have used $\gamma^2/gkA=1$ but have kept the same integration region $k_0\le k\le k_c$. This curve is higher because only one of the above two effects (limited integration range) is active to reduce $E_{\text{turbulent}}$ below the upper bound given in Eq. (43). Naturally, both curves are zero at $k_c/k_0=1$ and both approach $\frac{2}{3}(56/9\pi)^2\approx 2.6$ as $k_c/k_0\rightarrow\infty$. This upper curve can be found analytically:[18,20]

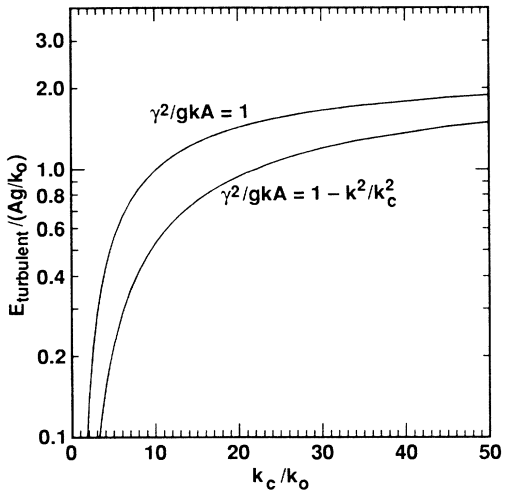

FIG. 9. Turbulent energy $E_{\text{turbulent}}$ in units of Ag/k_0 as a function of k_c/k_0 ($=\lambda_0/\lambda_c$), where λ_c is the cutoff wavelength and λ_0 is the largest wavelength present in the system. The lower curve labeled $\gamma^2/gkA = 1-k^2/k_c^2$ includes the reduction in the growth rate due to surface tension. The upper curve labeled $\gamma^2/gkA = 1$ is the tensionless case with a limited integration range and is given by Eq. (44). Both curves approach zero as $k_c/k_0 \to 1$ and they asymptote to $\frac{2}{3}(56/9\pi)^2$ as $k_c/k_0 \to \infty$.

$$E_{\text{turbulent}} = \frac{Ag}{k_0} \frac{[2+3k_0/k_c-5(k_0/k_c)^{3/4}]^3}{3\left[\frac{3\pi}{28}\right]^2 [3-10(k_0/k_c)^{7/4}+7(k_0/k_c)^2]^2} . \tag{44}$$

There is another practical interest in this curve having to do with experimental resolution. Surface tension may have been made small (for example, by using surfactants or fluids of naturally low surface tension) so that $\gamma^2 \approx gkA$ for all practical purposes, but the *experimental limit* on the smallest resolvable scale, say λ_c, may prevent one from including the turbulent energy in scales smaller than λ_c. Then one would use Eq. (44) to account for this experimental cutoff. Returning to the example mentioned above, if scales smaller than 1 mm cannot be resolved, then the "measured" turbulent energy would be only ~ 2000 ergs/g ($\sim 2Ag/k_0$ instead of $\sim 2.6Ag/k_0$).

In Ref. 18 we used the $E_p = E_k$ technique to estimate $E_{\text{turbulent}}$ (without surface tension) and assuming a linear density profile in the mixed region we obtained

$$E_{\text{turbulent}} = Agh/6 , \tag{45}$$

from which we determined

$$\lambda_0 = \frac{\pi}{2}\left[\frac{9\pi}{56}\right]^2 h \approx 0.40h , \tag{46}$$

in the Canuto-Goldman model. This is consistent with the qualitative description given earlier, viz., that the mixing width is controlled primarily by the larger scales which grow with time. The strict proportionality between λ_0 and h given in Eq. (46) implies that as h grows quadratically with time [see Eq. (38)] the largest wavelength grows similarly.

Combining Eq. (45) with Eq. (38) we get the time evolution of the turbulent energy:

$$E_{\text{turbulent}} = \frac{0.07}{6}(Agt)^2 . \tag{47}$$

A natural quantity to compare with $E_{\text{turbulent}}$ is what we call "directed energy" defined as $E_{\text{directed}} = \frac{1}{2}v^2 = \frac{1}{2}(gt)^2$. The ratio $E_{\text{turbulent}}/E_{\text{directed}}$ is therefore given by

$$E_{\text{turbulent}}/E_{\text{directed}} = \frac{0.07}{3}A^2 \approx 0.023A^2 . \tag{48}$$

We emphasize that Eqs. (47) and (48) do *not* depend on the Canuto-Goldman model [Eq. (46) does], and that they assume surface-tension effects to be negligible. A cutoff wave number, coming from physical surface tension or finite experimental resolution, can only reduce the turbulent energy (see Fig. 9), hence 0.023 appears to be an upper bound.

We hope that experimental measurements of $E_{\text{turbulent}}$ will soon be available. Equation (48) predicts that the ratio of turbulent to directed energy is independent of time and acceleration—a scaling that needs to be tested. The correlation of $E_{\text{turbulent}}$ with a cutoff wavelength induced by actual surface tension or experimental resolution as displayed in Fig. 9 would also be important. Finally, by changing fluids one would like to test the A^2 scaling given in Eq. (48).

VII. REVIEW, REMARKS, AND CONCLUSIONS

It was straightforward to incorporate the effects of surface tension in our general formalism and the result, Eq. (4), appears rather innocuous. However, the ease with which that equation was derived (hence we omitted the details) belies the rich phenomena associated with it: the consequences of surface tension turned out to be quite interesting as evidenced by the emergence of universal points and postshock oscillations. A breakthrough in our analysis of the $N=3$ case occurred when we found that the rather complicated expressions of Eqs. (13) and (14) could be described in a simple and general way (see Fig. 2) because the zeros could be located explicitly.

Our interest in surface tension is not purely mathematical. Water tank experiments need to account for $T^{(s)}$, whether it is for the study of single-scale perturbations or the multiscale turbulent region. Such experiments bear on the issues of density gradient stabilization, feed through of perturbations from one interface to another, and the loss of useful directed energy to turbulent energy, issues relevant for inertial confinement fusion (ICF) where accelerations are some 10^{13} orders of magnitude larger and where it becomes increasingly difficult to verify the answers to such questions. In addition, ablation and surface tension both stabilize the shorter-wavelength perturbations (each in its own regime), so one can use surface tension as a *model* for studying the effects of abla-

tive stabilization, always keeping in mind that extrapolations over so many orders of magnitude must be done with extreme care.

Another classical stabilization mechanism is of course viscosity, which we have neglected here. The treatment of viscosity is substantially different (and more difficult—see, e.g., Chandrasekhar[11]) from the treatment of surface tension because viscosity is a fluid property as opposed to surface tension, which is an interface property. We hope to include the effects of viscosity in a future work.

Going beyond the classical $N=2$ system, we expect a variety of new phenomena in 3-fluid experiments. The simplest phenomenon is inversion symmetry; for example, the growth rates in the profile $(\rho_1,\rho_2,\rho_3)=(1,5,10)$ are the same as in (1,2,10). Since surface tension spoils inversion symmetry, one should look for inversion symmetry with relatively long wavelengths (or, equivalently, use surfactants to reduce $T^{(s)}$). There is a second reason for preferring long wavelengths when verifying inversion symmetry, and this has to do with the decoupling of the two interfaces: short-wavelength perturbations are controlled by the local Atwood numbers at each interface, and these numbers are clearly invariant under inversion, hence the symmetry is trivial. These two reasons imply that the wavelength λ of the perturbation must satisfy $\lambda \gg \lambda_c$ and t (thickness of the middle layer) for interesting experiments of this nature. We emphasize that only the eigenvalues and *not* the eigenfunctions are invariant under inversion (see Ref. 6).

Taylor's case ($\rho_1=\rho_3=0$) is unfortunately difficult to set up experimentally: water tank experiments require a uniformly increasing density profile in the earth's gravitational field. This requirement on the density profile becomes an asset, rather than a liability, when it comes to studying universality: $\partial\rho/\partial y>0$ is in fact required for universality on a purely mathematical basis and not just experimental convenience, a happy coincidence. The (proposed) JC experiments come close to this situation with $0=\rho_1<\rho_2<\rho_3$, as we discussed in Sec. IV. The case is similar for the BSY experiments, which have a universal point at $\lambda=0.23$ cm. We hope $N=3$ water tank experiments will be carried out to study issues such as universality, density gradient stabilization, and feed through of perturbations from one interface to another.

Shocks at fluid interfaces with surface tension turned out to have interesting consequences. As we described in Sec. V, the reason is that shocks impact a kick $\dot{\eta}_0$ proportional to the wave number k, while surface tension induces oscillations having a frequency ω proportional to $k^{3/2}$, and the amplitude of the oscillations is $\dot{\eta}_0/\omega \sim k^{-1/2}$. We hope these predictions will also be tested experimentally, either as the time evolution of a single wavelength or of a spectrum of wavelengths. Let us mention that if the initial spectrum is not flat, one still uses Eq. (29) to advance each component; given the initial spectrum $\eta_0(k)$, the spectrum at any later time t is determined by $\eta(t,k)$ given in Eq. (29).

Our treatment was essentially incompressible, following Richtmyer's work to absorb the effects of compressibility into the amplitude η_0 and Atwood number A. Of course, Eq. (29) becomes exact in a truly incompressible experiment such as a water tank that is impulsively accelerated or decelerated. There is no need to limit Eq. (27) to impulsive accelerations only: if $g(t)$ is a time varying acceleration, then $\eta(t)$ still obeys the second-order differential equation

$$\frac{d^2\eta}{dt^2}=\gamma^2\eta=[g(t)kA-\omega^2]\eta(t)\ . \tag{49}$$

This equation can be used to study how perturbations evolve in fluids undergoing an arbitrary time-dependent acceleration $g(t)$. The constant acceleration $g(t)=g$ and the impulsive acceleration $g(t)=\Delta v\,\delta(t)$ are two simple (yet important) cases where Eq. (49) can be solved analytically.

Finally, we believe there is a wealth of information to be gained by carrying out experiments on turbulent mixing layers in accelerating fluids. Concepts based on linear and single-wavelength perturbations fail in this regime. To meet the challenge, we had to resort to one or more models in making the predictions of Sec. VI. It is highly probable that in the long run the *questions* raised in that section will be more useful than the tentative answers provided there.

Except for the experimental result $h=0.07Agt^2$, practically all the predictions made in Sec. VI beg for verification. The turbulent energy is an obvious candidate. Its dependence on a cutoff, displayed in Fig. 9, is based on the Canuto-Goldman model, where the cutoff can be physical (due to surface tension) or experimental (due to finite resolution) as shown by the two curves of Fig. 9. Such tests of the model are important because we wish to scale it to ICF regimes where measurement of $E_{\text{turbulent}}$ becomes extremely difficult, if not impossible, as discussed in Ref. 20.

Our arguments based on the conversion of potential energy to kinetic turbulent energy have perhaps a more secure footing. Assuming a linear density profile, we derived Eqs. (47) and (48), which imply that $E_{\text{turbulent}}$ is approximately equal to a few percent of E_{direct}. This result, for example, would scale to ICF regimes without change (if anything, ablation might reduce $E_{\text{turbulent}}$) implying that no more than a few percent of the absorbed laser energy can be lost to turbulence—a welcome result indeed. Obviously, such predictions will have to be abandoned if they are found to fail in much easily diagnosed water tank experiments.

In addition to serving as an upper limit Eqs. (47) and (48) suggest that we study the scaling of $E_{\text{turbulent}}/E_{\text{directed}}$ with A, g, and t separately. Clearly, one cannot justify extending our results to the ICF regime unless such scaling is well in hand.

We conclude with a call for not only physical experiments, which naturally have the final word, but also for numerical experiments. Several code calculations[22] have simulated mixing by the Rayleigh-Taylor instability, albeit without surface tension. It appears that with a little more effort one can throw light computationally on several if not all of the issues raised in this paper—the evolution of λ_0 with time (is $\lambda_0\approx 0.4h$ a valid approximation?), average density profile in the mixed region (is it

linear?), $E_{\text{turbulent}}$ (is it equal to $Agh/6$) and, finally $E_{\text{turbulent}}/E_{\text{directed}}$ (is $0.023A^2$ a valid approximation, and is there no g or t dependence?). We hope our predictions will soon be confronted with numerical or, better yet, actual physical experiments.

ACKNOWLEDGMENTS

This research was supported by the U.S. Department of Energy under Contract No. W-7405-ENG-48.

[1]Lord Rayleigh, *Scientific Papers* (Dover, New York, 1965), Vol. 2.

[2]G. I. Taylor, Proc. R. Soc. London, Ser. A **201**, 192 (1950).

[3]R. D. Richtmyer, Commun. Pure Appl. Math. **13**, 297 (1960).

[4]E. E. Meshkov, Izv. Akad. Nauk SSSR, Mekh. Zhidk. Gaza **5**, 151 (1969).

[5]R. Bellman and R. H. Pennington, Quart. Appl. Math. **12**, 151 (1954).

[6]K. O. Mikaelian, Phys. Rev. Lett. **48**, 1365 (1982); Phys. Rev. A **26**, 2140 (1982).

[7]The same happens with viscosity—see, e.g., P. Mulser, Laser Part. Beams **6**, 119 (1988).

[8]J. Nuckolls, L. Wood, A. Thiessen, and G. Zimmerman, Nature **239**, 139 (1972).

[9]K. D. Burrows, V. S. Smeeton, and D. L. Youngs, Atomic Weapons Establishment Report No. O22/84, 1984 (unpublished).

[10]J. W. Jacobs and I. Catton, J. Fluid Mech. **187**, 353 (1988).

[11]S. Chandrasekhar, *Hydrodynamic and Hydromagnetic Stability* (Oxford University Press, London, 1968).

[12]We found this property first in our study of RT and RM instabilities in spherical geometry where it appears as symmetry under $n \rightarrow -n-1$, n being the mode number of the spherical perturbation [K. O. Mikaelian, Phys. Rev. Lett. **65**, 992 (1990)].

[13]D. Besnard (private communication).

[14]*Handbook of Chemistry and Physics,* 68th ed. (CRC, Boca Raton, FL, 1988).

[15]References to early and recent work can be found in *Proceedings of the Princeton Workshop on the Physics of Compressible Turbulent Mixing,* Vols. I and II of *Springer Verlag Series Lecture Notes in Engineering,* edited by W. T. Dannevik, A. C. Buckingham, and C. E. Leith (Springer Verlag, Berlin, 1989).

[16]K. O. Mikaelian, Phys. Rev. A **31**, 410 (1985).

[17]K. I. Read and D. L. Youngs, Atomic Weapons Establishment Report No. O11/83, 1983 (unpublished); K. I. Read, Physica D **12**, 45 (1984).

[18]K. O. Mikaelian, Physica D **36**, 343 (1989).

[19]V. M. Canuto and I. Goldman, Phys. Rev. Lett. **54**, 430 (1985).

[20]K. O. Mikaelian, J. Appl. Phys. **65**, 964 (1989).

[21]S. A. Orszag, in *Fluid Dynamics* edited by R. Balian and J. L. Peube (Gordon and Breach, New York, 1977).

[22]For a review see D. H. Sharp, Physica D **12**, 3 (1984). Recent work includes J. A. Zufiria, Phys. Fluids **31**, 440 (1988); C. L. Gardner, J. Glimm, O. McBryan, R. Menikoff, D. H. Sharp, and Q. Zhang, *ibid.* **31**, 447 (1988); J. Glimm and X. L. Li, *ibid.* **31**, 2077 (1988); D. L. Youngs, Physica D **37**, 270 (1989).